OPEN ACCESS

Water Treatment Technologies ARTICLE

The Innovation Water

Novel high-density dynamic membranes break the energy-space trade-off in next-generation membrane bioreactor systems (MBRs)

Yanqing Zhang,[1,6] Yuxiang Liang,[2,6] Ying Chen,[3] Zhesong Zhou,[4] Pingli Li,[2] Dongqing Zhan,[2] Chenxuan Lou,[2] Yangcheng Ding,[2] Yijing Xia,[1] Wei Sun,[2] Yao Feng,[2] Jionghui Li,[2,*] and Huajun Feng[1,2,5,*]

*Correspondence: fenghuajun@zafu.edu.cn (H.F.); Lijionghui@zafu.edu.cn (J.L.)

Received: April 10, 2026; Accepted: August 18, 2026; Published Online: August 18, 2026; https://doi.org/10.59717/j.tiw.2026.100012

GRAPHICAL ABSTRACT

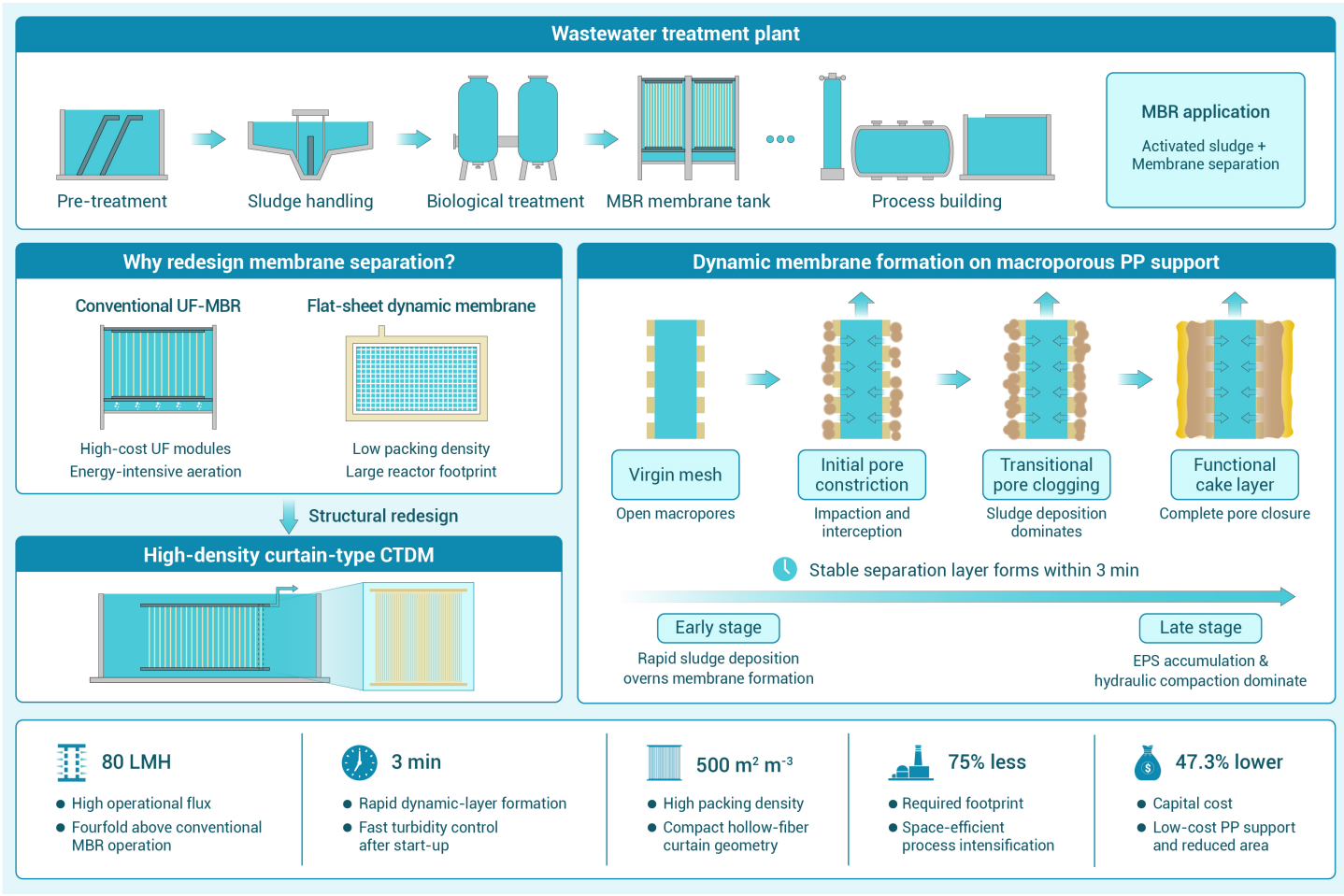

PUBLIC SUMMARY

- 73 h stable operation at 19 LMH, compared with 5 h for the initial operating period.
- Effluent turbidity fell below 10 NTU within 3 min and below 5 NTU within 30 min.
- Maximum tested CTDM flux reached 80 LMH, versus 15 LMH for the PVDF control.
- High-density geometry provided about 500 $m^2 \cdot m^{-3}$ membrane area and an estimated 47.3% CAPEX reduction.
- Pilot operation with municipal sewage verified technical feasibility.

ARTICLE Water Treatment Technologies

OPEN ACCESS

Novel high-density dynamic membranes break the energy-space trade-off in next-generation membrane bioreactor systems (MBRs)

Yanqing Zhang,[1,6] Yuxiang Liang,[2,6] Ying Chen,[3] Zhesong Zhou,[4] Pingli Li,[2] Dongqing Zhan,[2] Chenxuan Lou,[2] Yangcheng Ding,[2] Yijing Xia,[1] Wei Sun,[2] Yao Feng,[2] Jionghui Li,[2,*] and Huajun Feng[1,2,5,*]

[1]School of Environmental Science and Engineering, Zhejiang Gongshang University, Hangzhou 310018, China

[2]College of Environment and Resources, College of Carbon Neutral, Zhejiang Agriculture and Forestry University, Hangzhou 311300, China

[3]Zhejiang Bainuo Digital Intelligence Environmental Technology Co., Ltd., Hangzhou 310061, China

[4]Hangzhou Hua JIA Chi Environmental Protection Technology Engineering Co., Ltd., Hangzhou 310000, China

[5]Sino-Spain Joint Laboratory for Agricultural Environment Emerging Contaminants of Zhejiang Province, Hangzhou 311300, China

[6]These authors contributed equally

*Correspondence: fenghuajun@zafu.edu.cn (H.F.); Lijionghui@zafu.edu.cn (J.L.)

Received: April 10, 2026; Accepted: August 18, 2026; Published Online: August 18, 2026; https://doi.org/10.59717/j.tiw.2026.100012

Citation: Zhang Y., Liang Y., Chen Y., et al. (2026). Novel high-density dynamic membranes break the energy-space trade-off in next-generation membrane bioreactor systems (MBRs). *The Innovation Water* **1**:100012.

Membrane bioreactors (MBRs) are pivotal for advanced wastewater treatment, yet conventional ultrafiltration membranes face challenges of high cost, energy-intensive operation, and limited flux. The emerging dynamic membrane filtration technology in recent years addresses these limitations, but flat-sheet dynamic membranes still face challenges in engineering applications due to their large footprint. This study introduces a novel hollow fiber curtain-type dynamic membrane (CTDM) fabricated from polypropylene (PP), designed to overcome these limitations. At a flux of 19 $L{\cdot}m^{-2}{\cdot}h^{-1}$(LMH), the CTDM presents excellent hydraulic stability, with its steady operating duration extended 14 times (73 h vs. 5 h). It also achieves rapid turbidity removal: the effluent turbidity decreases to below 10 NTU within 3 minutes, drops below 5 NTU within 30 minutes, and further falls to less than 3 NTU within 60 minutes. Scale-up experiments using domestic sewage validated the technical feasibility of the CTDM. From an engineering economics perspective, the CTDM achieves 47.3% capital cost reduction compared to conventional MBR systems through enhanced space efficiency (500 $m^2{\cdot}m^{-3}$ vs. < 200 $m^2{\cdot}m^{-3}$ reactor volume). This study provides theoretical and practical support for the engineering application of dynamic membrane and is expected to promote the further development of MBR technology.

INTRODUCTION

Membrane Bioreactors (MBRs) have emerged as a pivotal innovation in wastewater treatment, seamlessly integrating biological degradation with membrane separation to achieve effluent quality surpassing conventional processes.[1] With a global market projected to reach $7.15 billion by 2029,[2] MBRs are increasingly deployed for their ability to decouple sludge and hydraulic retention times while producing ultralow-turbidity effluent (< 0.5 NTU). However, widespread adoption is hampered by persistent challenges: energy-intensive fouling control, frequent chemical cleaning, and the high capital cost of ultrafiltration (UF) membranes.[3] These limitations underscore an urgent need for scalable, cost-effective alternatives that retain the core advantages of MBRs while mitigating their operational inefficiencies.

Dynamic membranes (DMs), formed in situ by the deposition of biomass and particulates onto porous substrates, present a compelling solution to these barriers.[4] Early pioneering work by Fan and Huang established the feasibility of self-forming dynamic membranes (SFDMs) in municipal wastewater treatment, demonstrating that in situ cake layers can act as effective selective barriers without the need for expensive UF materials.[5] Subsequent studies have shown SFDMs can achieve fluxes of 30-50 $L{\cdot}m^{-2}{\cdot}h^{-1}$ (LMH) with inherent antifouling properties, as the reversible cake layer avoids the irreversible pore clogging common in conventional UF membranes.[6] However, conventional flat-sheet DM configurations face a critical scalability barrier: packing densities rarely exceed 200 $m^2{\cdot}m^{-3}$, necessitating impractical large reactor footprints.[5,6] This spatial inefficiency contrasts starkly with commercial hollow fiber UF modules, which achieve packing densities of ~500 $m^2{\cdot}m^{-3}$ but have not been adapted for DM applications due to the lack of compatible low-cost substrates.

Recent advances have highlight substrate pore size (20-30 μm) as a key determinant of DM performance, balancing permeability and cake layer stability.[6-8] While stainless steel or ceramic substrates offer mechanical robustness, they often suffer from unstable biofilm adhesion and metal ion leaching (e.g., Fe^{3+}, Al^{3+}) that disrupts microbial community structure.[8] Polymeric alternatives such as nylon nonwovens require costly hydrophobic modifications to avoid premature wetting and maintain permeability,[9] eroding their cost advantage. Polypropylene (PP) is a promising candidate due to its chemical inertness, resistance to oxidative damage, low material cost, and intrinsic hydrophobicity that minimizes non-specific organic adsorption. However, PP-based substrates remain underexplored in high-density DM configurations, with no systematic evaluation of their performance in pilot-scale MBR systems. Bridging this gap, our study introduces a high-density hollow fiber curtain-type dynamic membrane (CTDM) engineered for rapid cake formation, robust hydraulic performance, and minimal spatial demands. Through advanced characterization (filtration resistance modeling, XDLVO interfacial theory) and multi-scale trials from benchtop to 20 t/d pilot, we elucidate the interplay between substrate properties, fouling mechanisms, and process scalability relative to prior DM designs.

This study not only validates the technical feasibility of PP-based CTDM but also quantifies their economic viability, demonstrating a 47.3% CAPEX reduction and 75% footprint savings compared to traditional UF-MBR systems. By resolving the long-standing trade-off between energy efficiency and spatial optimization in DM technology, our findings pave the way for next-generation MBRs capable of meeting escalating global wastewater treatment demands sustainably.

MATERIALS AND METHODS

Membrane module fabrication

Three scales of CTDM membrane modules were employed in this study, namely small-, medium-, and large-scale modules. All modules were made of polypropylene (PP) hollow fibers with a nominal pore size of 200 μm and assembled into curtain-type structures. The small-scale module consisted of 4 fiber cords (15 cm in length) with a total effective surface area of $3.8{\times}10^{-3}$ m^2. The medium-scale module comprised 36 fiber cords (30 cm in length), giving an effective surface area of $6.8{\times}10^{-2}$ m^2. The large-scale module was assembled from 5 sets of 36 fiber cords (50 cm in length), with a total effective surface area of 0.57 m^2.

For comparison, a commercial polyvinylidene fluoride (PVDF) ultrafiltration (UF) membrane with a nominal pore size of 0.1 μm was used. The membrane was purchased from Hangzhou Tianchuang Environmental Technology Co., Ltd., under the model number EM-MBR-PVDF-20. This PVDF membrane was fabricated into a small-scale module (denoted as PM) with the same dimensions and effective surface area as the small-scale CTDM module.

All membrane modules were potted in custom-made polypropylene sleeves. One end was sealed with epoxy resin adhesive (RILIK®, cured at 25°C for 24 h), while the other end remained open. Given the specific characteristics of the large-scale CTDM module, an aluminum plate was bonded to its bottom to provide sufficient gravity for submersion, preventing flotation

above the sludge mixture in the pilot-scale wastewater treatment plant. A flow control valve was installed at the permeate outlet to regulate and control the flux.

Experimental setup and operational conditions

Laboratory small-scale equipment and operation conditions. A 1.5-L acrylic reactor (15 × 7 × 20 cm) was equipped with a 0.2 μm microporous aerator to maintain the dissolved oxygen level at 3-5 mg·L^{-1} via continuous aeration (max 4 L·min^{-1}) (SB-988, SOBO) (Figure S2). Effluent flow and reactor level were regulated by peristaltic pumps (REWAY PUMP BS100A), ensuring steady hydraulic retention time (HRT: 12 hours). Transmembrane pressure (TMP) was monitored in real-time using a digital pressure transmitter (Asmik MIK-P300; ±0.5% FS accuracy), with data logged via a custom interface.

Activated sludge was sourced from Yuhang Wastewater Treatment Plant (Hangzhou, China). The reactor maintained mixed liquor suspended solids (MLSS) at 3,500±500 mg·L^{-1}, with the temperature of 25±2°C. This study used synthetic sewage (composition in Tables S1- S2) for small-scale CTDM tests.

Three flux conditions (19, 38 and 80 LMH) were tested in duplicate. Wastewater was fed continuously, and TMP was monitored in real time by the pressure transmitter. Effluent samples were collected at 0, 3, 6, 10, 20, 30 and 60 minutes, as well as when TMP reached 0.01, 0.02, 0.03 and 0.04 MPa. When the TMP reached 0.04 MPa, the operation was terminated. The filter cake layer on the surface of the membrane was scraped off and dissolved in 100 mL of pure water (ultrasonic treatment at 25°C for 10 minutes) for analysis. Detailed operating parameters for small, medium and pilot-scale MBR systems are compiled in Table S3.

Laboratory medium-scale equipment and operation conditions. An acrylic cylindrical reactor with an effective volume of 50 L (height: 1 m; diameter: 8 cm) was adopted. Consistent with the configuration of the laboratory small-scale setup described in Laboratory small-scale equipment and operation conditions section, the sludge source and cultivation method were kept identical. Actual domestic sewage was used as the influent, and continuous operation was conducted for one week under two flux conditions (15 LMH and 80 LMH) with an HRT of 12 h. Samples were collected every 24 h for subsequent water quality determination. The actual domestic sewage used in the experiment was collected from Phase IV of Yuhang Wastewater Treatment Plant in Hangzhou.

In continuous experiments, start the backwashing operation when the TMP reaches the threshold of -0.04 MPa. For execution, the membrane module was first detached from the reactor, followed by gentle physical brushing with a soft nylon brush to dislodge entangled sludge flocs and foreign debris from the fiber surface without damaging the PP substrate. The module was then rinsed thoroughly with clean tap water until no visible residual solids remained, before being reinstalled into the reactor to resume normal operation. This manual protocol mirrors the principles of automated mechanical brushing—an established and fully adaptable engineering solution for cleaning within curtain-type membrane spacings. TMP data were recorded during operation, and water samples were collected every 24 hours to determine conventional indicators such as turbidity, COD, ammonia nitrogen, and total phosphorus.

Pilot-scale plant and operation conditions of wastewater treatment plant. The pilot-scale plant was deployed at Phase IV of the Yuhang Wastewater Treatment Plant (Hangzhou, China), featuring a nominal treatment capacity of 20 m^3/d. To ensure alignment with full-scale operational realities, the system treated raw municipal sewage directly extracted from the plant's influent channel. An integrated AAO+MBR process was employed, comprising an equalization tank, anaerobic tank, anoxic tank, aerobic tank, and membrane tank. Crucially, the commercial MBR modules were replaced with the large-scale CTDM modules developed in this study to evaluate their field performance.

The system operated continuously under typical municipal conditions. The total Hydraulic Retention Time (HRT) was maintained at 12 h, with a phased distribution as follows: 2 h (anaerobic), 3 h (anoxic), 6 h (aerobic), and 1 h (membrane tank). The Mixed Liquor Suspended Solids (MLSS) concentration in the aerobic tank was controlled at 3,300 ± 200 mg·L^{-1} by daily discharge of approximately 2.6 kg of dry sludge. Aeration intensity in the MBR tank was fixed at 60 $Nm^3 \cdot m^{-2} \cdot h^{-1}$ (calculated based on the projected area of membrane modules). To assess flux-dependent performance, the CTDM was operated under three sequential phases: 15 LMH for five cycles, 25 LMH for six cycles, and 75 LMH for five cycles. This was achieved by proportionally increasing the influent flow rate to compensate for the higher filtration velocity. Consequently, while the per-cycle filtration time decreased at higher fluxes, the overall hydraulic residence time within the bioreactor remained constant, ensuring that biological treatment efficiency was not confounded by hydraulic variations.

Operational TMP data were acquired continuously; upon reaching the threshold of -0.04 MPa, the backwashing procedure described in Laboratory medium-scale equipment and operation conditions section was implemented. Effluent samples were taken every 2-3 days (depending on actual operating conditions) to determine conventional indicators such as turbidity and particle size. At the end of the 3rd cycle in the middle of each flux operation phase, sludge samples were scraped from the surface of the CTDM membrane for subsequent determination of EPS content. In addition, to track the structural stability of the membrane during operation, membrane samples were collected from the CTDM system at the initial and final stages, and material characterization was performed to evaluate the structural stability of the CTDM.

Analytical techniques

Membrane characterization. Morphology: A suitable portion of the membrane sample was affixed directly onto conductive adhesive. Subsequently, gold sputtering was performed using a Quorum SC7620 sputter coater at a current of 10 mA for a duration of 45 s. Following gold coating, the surface morphology of the membrane samples was examined and imaged using a ZEISS GeminiSEM 360 scanning electron microscope.

Surface chemistry: Fourier transform infrared (FTIR) spectra were acquired using a Thermo Fisher Scientific Nicolet iS20 spectrometer over a wavenumber range of 4,000-400 cm^{-1}, with a spectral resolution of 4 cm^{-1} and 32 co-added scans. Surface elemental composition was determined utilizing X-ray photoelectron spectroscopy (XPS; Thermo Scientific K-Alpha), identifying predominant elements including carbon, oxygen, and fluorine. The spectra were obtained using an Al Kα X-ray source (1,486.6 eV), and binding energies were rigorously calibrated against the C 1s peak at 284.8 eV.

Hydrophilicity: Contact angles were measured using a Kunshan Shengding SDC 350KS goniometer. To determine the various surface tension components of the solid surface, three standard probe liquids—ultrapure water, glycerol, and n-hexadecane—were employed. The parameters for testing liquid surface tension are shown in Table S4. A 2 μL droplet was dispensed for each measurement, and the dynamic evolution was monitored for 60 s. The equilibrated contact angle values at the 60-second mark were utilized for subsequent calculations.

Porosity: Prior to analysis, samples were degassed under vacuum using a Micromeritics SmartVacPrep degassing station at 120°C for 12 h. Nitrogen adsorption–desorption isotherms were subsequently collected at 77 K using a Micromeritics ASAP 2460 four-port automated surface area and porosity analyzer. The specific surface area and pore structure parameters were calculated from the obtained isotherms using the Brunauer–Emmett–Teller (BET) model.

Zeta potential: Zeta potentials of the membrane surfaces were measured using a Thermo Scientific K-Alpha solid-surface Zeta potential analyzer. Prior to testing, membrane samples were trimmed to appropriate dimensions and secured in the sample cell. A 0.001 mol·L^{-1} NaCl aqueous solution was employed as the background electrolyte, and all measurements were performed at room temperature. The solid-surface Zeta potential was recorded at a fixed pH of 7.0.

Effluent and sludge analysis. Water quality: Chemical oxygen demand (COD), ammonium (NH_4^+), total phosphorus (TP), and turbidity were analyzed by standard methods.[10] Fecal coliforms were determined by Zhejiang Hongbo Environmental Testing Co., Ltd. using the Paper Strip Rapid Method (HJ 755-2015), with incubation performed at 44.5°C ± 0.5°C for 15 h in an SHP-250(D) biochemical incubator (Unit No. 083). Effluent samples were filtered through 0.22 μm syringe filters. The pH was measured with a digital pH meter (Seven Direct SD20).

Particle size distribution: Effluent particle sizes were measured using an Anton Paar Litesizer 500 nanoparticle size analyzer. Prior to measurement, samples were thoroughly homogenized via vortexing and promptly aliquoted to minimize errors arising from particle sedimentation, then loaded into dedicated cuvettes for analysis. Triplicate measurements were performed for each sample, and the mean value was adopted as the final result to ensure data accuracy and reproducibility.

Three-dimensional fluorescence spectroscopy: Qualitative analysis of the effluent water quality was performed using a Hitachi F-4700 three-dimensional fluorescence spectrophotometer. Excitation (Ex) wavelengths were scanned from 220 to 450 nm, and emission (Em) wavelengths from 260 to 600 nm. The wavelength scan step size was set to 5 nm, with a scanning speed of 12,000 nm·min^{-1}. The photomultiplier tube (PMT) voltage was maintained at 700 V, and the response time was fixed at 0.05 s. All measurements were conducted at room temperature under conditions free from stray light interference.

Fluorescence microscopy: The CTDM formation process at constant flux was visualized by a fluorescence microscope (NIB-900). A small fragment was stained with 1 μL of LIVE/DEAD BacLight Bacterial Viability Kit (Beyotime Biotech C2030S) and incubated at 37°C in the dark for 15 minutes before observation.

Extracellular polymeric substances (EPS) analysis: Following membrane filtration, sludge cake was harvested and subjected to ultrasonic treatment for EPS fractionation.[11] First, samples were centrifuged using a refrigerated centrifuge (TGL-16M) at 6,000 rpm for 10 min at 4°C. The supernatant was filtered through a 0.22 μm membrane to obtain the soluble EPS fraction (SEPS). The remaining pellet was resuspended in phosphate buffer solution to restore the original volume. Bound EPS (BEPS) was subsequently extracted by heating the suspension at 60°C for 30 min, followed by centrifugation at 10,000 rpm for 20 min at 4°C. The resulting supernatant was filtered through a 0.22 μm membrane to yield the BEPS fraction.

Protein content in both fractions was quantified using the BCA assay (BCA Protein Assay Kit, Beyotime Biotech Inc, P0010S). Polysaccharide content was determined via the phenol-sulfuric acid method.[12] Specifically, 2.0 mL of sample was mixed with 1.0 mL of 6% phenol, followed by the rapid addition of 5.0 mL concentrated sulfuric acid. After thorough vortexing and a 30 min incubation at room temperature, absorbance was measured at 490 nm and correlated to a standard curve for concentration determination.

Filtration resistance modeling. Total resistance (R, m^{-1}) was calculated via Darcy's law:

$$J = \frac{TMP}{\mu R} \quad (1)$$

Where J is the permeate flux (LMH), TMP is the transmembrane pressure (kPa), μ is the dynamic viscosity of the filtrate (Pa·s), and R represents the total filtration resistance (m^{-1}). During the experiments, J was determined in real time by monitoring the mass of permeate using an electronic balance (NX3000, capacity 3 kg, accuracy ±0.01 g) connected to a data acquisition system. Flux was then calculated based on the measured mass, membrane surface area, and corresponding time interval. TMP was continuously monitored and recorded using the aforementioned online high-precision pressure transmitter. The μ of the supernatant obtained after settling the sludge mixture in the reactor was measured at the experimental temperature using a rotational viscometer (Brookfield DV3T).

Interfacial interaction analysis—XDLVO theory

The XDLVO theory extends the classical Derjaguin-Landau-Verwey-Overbeek (DLVO) framework by incorporating Lewis acid-base (AB) interactions alongside van der Waals (LW) and electrostatic double-layer (EL) effects.[13] It is typically applied to interactions between smooth planar surfaces; the total interaction energy is expressed as:

$$U^{TOT} = U^{LW} + U^{EL} + U^{AB} \quad (2)$$

Where U^{TOT} is total interaction energy, U^{LW} is LW free energy, U^{EL} is EL free energy, U^{AB} is AB interaction energy. Derivations and computational details for each energy component are provided in Text S1.

Construction of predictive model methods

Historical data mainly cover the period from 2011 to 2024. Data regarding the operational scale of MBR processes and the production scale of MBR membranes in China are primarily sourced from reports released by a market consulting institute (https://www.gonyn.com). Meanwhile, specific operational data and characteristic parameters of MBR processes are comprehensively compiled from published academic literature[14] and field operational records of wastewater treatment plants affiliated with Yuhang Water Group in Hangzhou, Zhejiang Province, China, which guarantees the reliability and representativeness of the historical dataset.

The future trend forecasting targets the upcoming decade spanning 2025 to 2035. Quantitative models are adopted for projection. Based on distribution analysis of historical data, the forecasting function embedded in Oracle Crystal Ball software is employed, and the optimal non-seasonal, non-stochastic simulation algorithm is selected. A total of 100 independent simulation runs is conducted to secure stable and convergent forecasting outputs. Detailed configurations of forecasting function models, relevant parameters, and simulation results are summarized in Tables S5-S7.

RESULTS AND DISCUSSION

Membrane structure innovation: Polypropylene curtain architecture for rapid self-organization

The material used for the CTDM in this study (PP fiber rope) is normally used as an internal support frame for the PM. Therefore, the physicochemical characteristics of the CTDM and PM were systematically compared to elucidate their distinct filtration behaviors. FTIR confirmed the chemical composition of the CTDM, dominated by C-H and C=O bonds characteristic of PP (Figure 1A), while XPS revealed carbon (84.2 at%) and oxygen (15.8 at%) as primary surface elements, with no detectable fluorine—a critical advantage over fluoropolymer-based membranes prone to oxidative degradation (Figure 1C). As evidenced by the pore architecture characterization (Figure 1B), the CTDM exhibited a significantly reduced porosity profile relative to the PM. While this structural divergence could marginally compromise initial filtration flux efficiency, it simultaneously mitigated particulate adsorption kinetics and suppressed membrane fouling propensity through enhanced surface selectivity.[15]

SEM highlighted the CTDM's interwoven fibrous structure (Figure 1D), creating a microscale roughness conducive to biofilm adhesion through mechanical interlocking.[16] In contrast, the PM exhibited a smoother surface, consistent with its ultrafiltration-grade fabrication. Hydrophilicity, a key determinant of fouling resistance, differed obviously between CTDM and PM, with apparent contact angle of 69°±1.3° and 90°±0.5°, respectively (Figure 1E). The low apparent contact angle of the PP CTDM stems from its macroporous fibrous structure rather than enhanced intrinsic hydrophilicity of PP. Capillary infiltration in inter-fiber voids reduces the macroscopic contact angle,[17] while smooth bulk PP has a contact angle of 100°-110°.[18] The dense PVDF membrane excludes capillary penetration, so its contact angle represents the intrinsic property of PVDF. This structural-induced wettability of CTDM benefits sludge adhesion and dynamic membrane formation.

This enhanced hydrophilicity promotes water permeation while mitigating organic adsorption, aligning with prior studies linking lower contact angles to reduced irreversible fouling.[19] Surface charge analysis further differentiated the two membranes. The CTDM's zeta potential (-39.54 mV) exceeded the PM's (-28.7 mV) in magnitude (Figure 1F), amplifying electrostatic repulsion against negatively charged sludge particles (-3.12 mV). [20] This electrostatic barrier likely delayed pore clogging, as evidenced by the CTDM's prolonged stable operation (Filtration performance: high-flux operation with ultrafast contaminate control section).

Flat-sheet DMs, often fabricated from stainless steel or nylon, face inherent limitations. Metallic substrates, despite high mechanical strength, suffer from biofilm detachment due to smooth surfaces and metal ion leaching (e.g., Fe^{3+}, Al^{3+}), which destabilize microbial communities.[21,22] Nonwoven fabrics, though porous, require costly hydrophobic modifications to achieve comparable flux.[23] The PP-based CTDM circumvented these issues through its inherent hydrophilicity, chemical inertness, and textured morphology, enabling stable operation in complex wastewater matrices without oxidative degradation—a common failure mode for nylon membranes.[24]

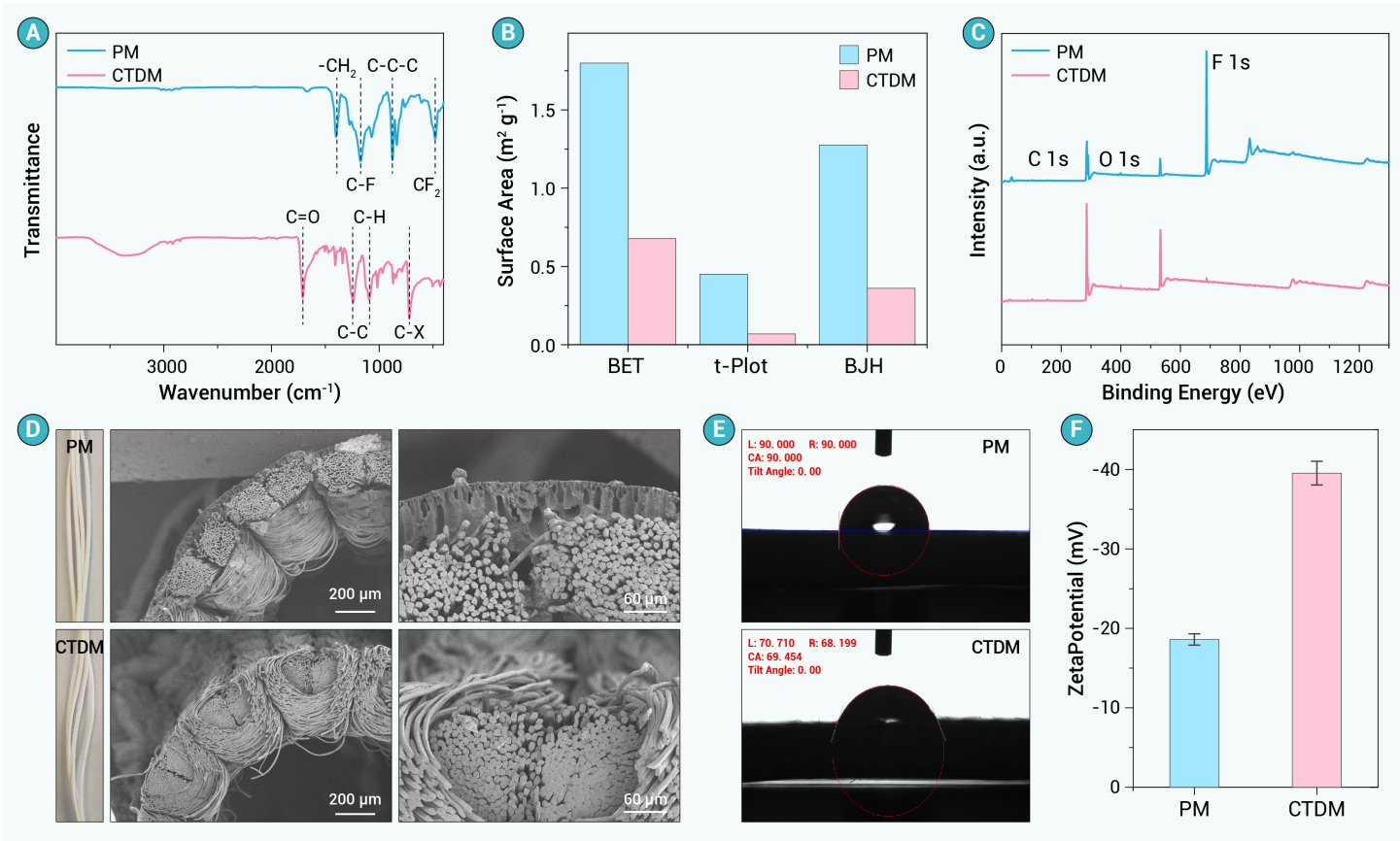

Figure 1. Physicochemical properties of PM and CTDM (A) FTIR spectra; (B) Specific surface areas and pore structure; (C) XPS full survey spectrum; (D) Digital photos and cross-sectional SEM images; (E) Contact angle test results; (F) Surface zeta potential.

These findings underscore the CTDM's material advantages: a synergy of hydrophilicity, surface charge, and structural robustness that positions it as a viable, low-cost alternative to conventional MBR membranes. By addressing the shortcomings of both flat-sheet DMs and commercial PVDF modules, the PP hollow fiber design bridges the gap between high performance and practical scalability.

Filtration performance: High-flux operation with ultrafast contaminate control

The CTDM demonstrated exceptional filtration performance across a spectrum of operational fluxes (19-80 LMH), outperforming both commercial PM and conventional flat-sheet DMs. At 19 LMH, the CTDM sustained stable operation for 73 h before reaching the critical TMP threshold (-0.04 MPa), a 14.6-fold improvement over the PM's 5 h lifespan (Figures 2A & C). Both CTDM and PM exhibited shorter operational durations with increasing flux, which is consistent with the mechanism that higher flux accelerates dynamic membrane formation yet simultaneously exacerbates transmembrane pressure buildup.[25] Notably, the CTDM flux performance (80 LMH) was significantly better than that reported in the literature for flat-sheet DMs (14.8-33.3 LMH). [5,26]

Regarding the rejection performance of the dynamic membrane (Figure 2B), the CTDM exhibited rapid cake layer formation. At all tested fluxes, the CTDM reduced effluent turbidity to below 10 NTU within 3 min of startup. Subsequently, with further compaction of the cake layer, effluent turbidity continued to improve and stabilized within 60 min. In contrast, owing to its dense external PVDF filtration layer, the PM maintained stable effluent turbidity below 5 NTU throughout operation, both at the initial stage and under elevated TMP conditions (Figure 2D). Although the initial effluent turbidity (20.03±6.96 NTU) exceeded that of the PM (3.72±1.26 NTU), the system stabilized rapidly within this short period. This transient phase is negligible in continuous operation, especially when recirculation or parallel module configurations are used. The rapid formation of a functional cake layer underscores the CTDM's suitability for applications requiring immediate effluent quality control, such as decentralized wastewater treatment.[27]

Notably, a negative correlation between operating flux and effluent turbidity was observed for the dynamic membrane, differing from results reported in prior literature.[28,29] In this work, higher fluxes (e.g., 80 LMH) accelerated the decline of effluent turbidity. Beyond enhanced shear forces that drive preferential deposition of large particles,[9] the special macroporous structure of the PP-based CTDM also promotes rapid compaction of the surface cake layer under high hydraulic load.[30] The synergism of hydrodynamic conditions and substrate structural features accounts for this unique variation trend of effluent turbidity. Nevertheless, at all operating fluxes, once TMP exceeded -0.02 MPa, microcrack propagation likely occurred within the cake layer, resulting in an instantaneous increase in turbidity (up to 20 NTU, Figure 3B). This observation aligns with the three-stage theory of dynamic membrane formation [24], in which excessive pressure compromises the structural stability of the mature cake layer. Accordingly, this phenomenon suggests that careful selection of operating flux and TMP is essential during CTDM operation. To strike a balance between high treatment efficiency, stable effluent quality and long-term operational reliability, a moderate flux range is recommended for practical use. Backwashing should preferably be conducted before TMP reaches -0.02 MPa, which effectively avoids cake layer cracking, prevents sharp rises in turbidity and ensures effluent meets discharge standards. Operating within this matched flux and TMP interval can maintain steady filtration performance and extend the service cycle of the CTDM system.

Moreover, effluent particle size distribution revealed the CTDM's superior retention efficiency. Under 19-38 LMH fluxes, the dominant particle size in the effluent stabilized at 100 nm after 60 minutes (Figure 3A), a fourfold reduction compared to the 400 nm particles reported in prior studies.[31] This rapid interception of organics contrasts sharply with the 6-8 days DM formation periods documented for flat-sheet systems,[6] underscoring the efficiency of the hollow fiber configuration under shear-enhanced hydrodynamic conditions.

Analysis of membrane surface deposits further elucidated the fouling characteristics under varying flux conditions. Experimental results showed that

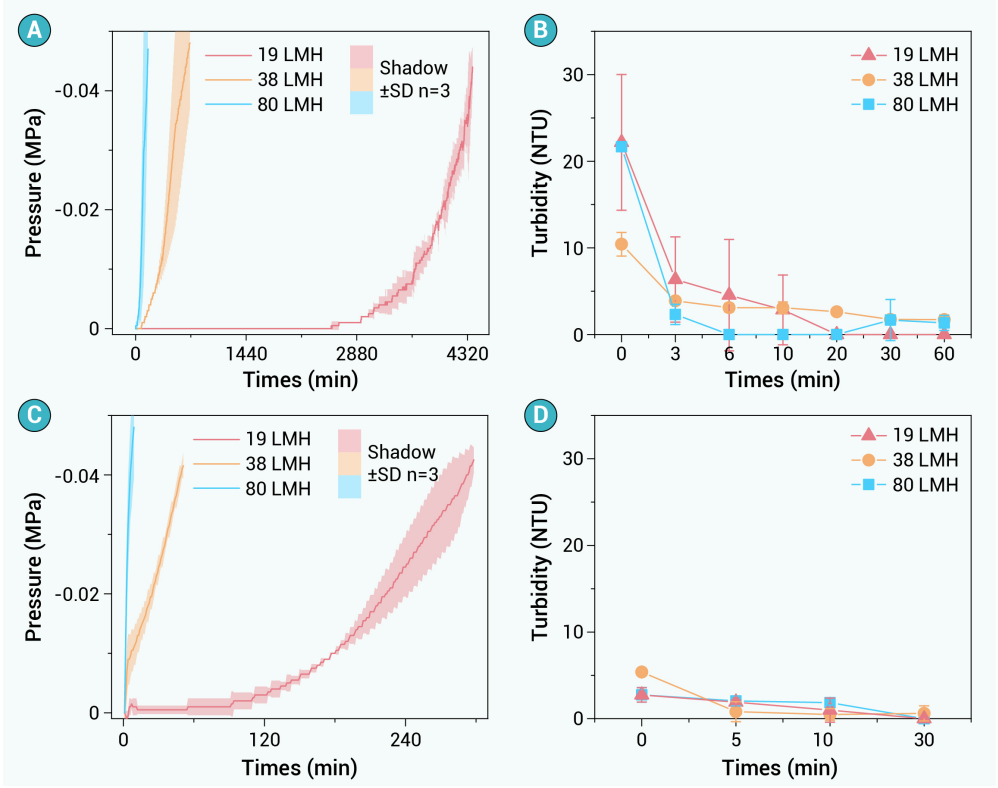

Figure 2. Variations in TMP and turbidity of PM and CTDM (A) TMP variation of CTDM; (B) Turbidity of CTDM; (C) TMP variation of PM; (D) Turbidity of PM.

after CTDM operation at 19, 38, and 80 LMH, the EPS content on the membrane surface was 97.4, 68.5, and 61.6 mg·L^{-1}, respectively, while the corresponding sludge loading was 4.0, 4.2, and 7.4 g·m^{-2}. These results indicate that operation at low flux (19 LMH) leads to a significant increase (35%-50%) in bound EPS on the CTDM surface, making it more susceptible to pore clogging (Figure 3C). In contrast, under high-flux conditions (80 LMH), sludge deposition rather than EPS accumulation becomes dominant, with the attached sludge mass increasing linearly with rising flux (Figure 3D). This trend is consistent with the fouling model based on transport dynamics proposed by Gholami,[32] confirming that sludge deposition represents the primary fouling mechanism of CTDM during high-flux operation. Collectively, CTDM exhibits distinct advantages of high flux and low fouling propensity, positioning it as a promising alternative to conventional membrane technologies.

Formation mechanism: Interfacial interaction-driven self-assembly and fouling dynamics

The dynamic formation process of CTDM was visualized using fluorescence microscopy (Figures 4B1-B4 & C1-C4), revealing three distinct stages: initial pore constriction, transitional pore clogging, and complete pore closure. A schematic illustration of the CTDM formation mechanism is provided in Figure 4A. In the first stage, the support matrix with an original pore size of approximately 200 μm began to capture sludge particles, resulting in a significant linear reduction in the effective pore diameter. This stage was mainly governed by inertial impaction and interception mechanisms in fluid mechanics, where large sludge flocs preferentially deposited at mesh junctions or grid edges. Chen et al. [21] also visually confirmed this phenomenon via morphological characterization, showing that the sludge mass attached to the substrate surface gradually increased with operating time.

During the second stage, the internal pores became substantially filled, leading to a nearly fully clogged state. The filtration resistance at this stage was primarily attributed to the physically deposited cake layer; although interparticle voids continued to narrow, the fluid pathways remained partially interconnected. Upon entering the third stage, however, complete pore closure occurred, accompanied by a sharp surge in EPS concentration from an initial 32.05 mg·L^{-1} to 135 mg·L^{-1}, representing an increase of up to 321%. This dramatic change triggered an exponential rise in TMP. These observations are consistent with the theory proposed by Liu et al. [33,33], who emphasized that EPS acts as a key contributor to hydraulic resistance in the late fouling stage. Similarly, the study by Chu et al. [22] reported a TMP profile characterized by a gradual initial increase followed by a sharp rise, which aligns well with the trend observed in the present work.

To further mechanistically elucidate the formation and fouling processes of CTDM, this study investigated the interrelationships among TMP, sludge deposition mass, and EPS secretion (Figures S4D-F). It was found that, at the initial stage of operation with TMP below -0.01 MPa, the amount of sludge deposited on the membrane surface increased rapidly from 88.9 mg·L^{-1} to 406.2 mg·L^{-1}, representing a 357% increment (Figure S3), whereas the EPS concentration fluctuated slightly with a relative change of < 7.2%. These results clearly demonstrate that the deposition of sludge particles serves as the dominant mechanism governing the initial formation of the dynamic membrane. As TMP continued to rise beyond -0.01 MPa, the EPS concentration surged sharply from 34.4 mg·L^{-1} to 135 mg·L^{-1} within a short period, showing a 293% increase. In comparison, the membrane-surface sludge deposition only increased by 40%. This observation indicates that membrane fouling in the later operational stage is primarily driven by the massive secretion and accumulation of EPS. The pore-clogging and adsorptive effects of EPS gradually replace sludge deposition as the key factor controlling the operational stability of the dynamic membrane.

Interfacial energy analysis based on the XDLVO theory quantified the asymmetric forces governing CTDM assembly (Figure 5). [34,35] For membrane-sludge interactions (Figures 5A1-A4), AB attraction (-1.54×10^{-14} J) outweighed LW repulsion (5.63×10^{-16} J) by 27-fold, consistent with PM fouling.[36] Conversely, sludge-sludge interactions (Figures 5B1-B4) exhibited dominant AB attraction (-1.11×10^{-14} J) and negligible EL repulsion (< 1.70×10^{-18} J), driven by the stark zeta potential disparity between membrane (ζ = -39.54 mV) and sludge (ζ = -3.121 mV). This unique energy gradient lowers interfacial barriers and accelerates particle adhesion, enabling the CTDM to form a stable filtration layer within 3 minutes — a significant improvement over earlier systems that took 3 days,[37] 7 hours,[31] and 45 minutes.[38] This core mechanism has been validated by Zamani et al., [39] and XDLVO theory is widely used to guide the surface modification of membrane substrates. As typical examples, supramolecular hydroxyl clusters can tune interfacial forces to reach a BSA rejection rate above 97%,[40] while polydopamine coating modulates surface negative charges following XDLVO rules and reduces protein adsorption by 50% in municipal wastewater.[41] These surface engineering methods that regulate interfacial energy to resist fouling are also reflected in the modification strategies proposed by Li et al. [42]

The above results indicated that the formation of the CTDM is essentially a physical-chemical coupling process dominated by interfacial interactions. In the initial stage, the strong AB interaction between the membrane and the sludge drives the rapid adsorption of particles. As the operating pressure increases, the shear-induced secretion of EPS exacerbates the pore clogging. Finally, the construction of the CTDM is completed through the complete blocking. This mechanism analysis provides an important theoretical basis for optimizing the process parameters of DMs.

Engineering viability: Demonstrated scalability and techno-economic advantage

The engineering feasibility of CTDM was systematically verified through a

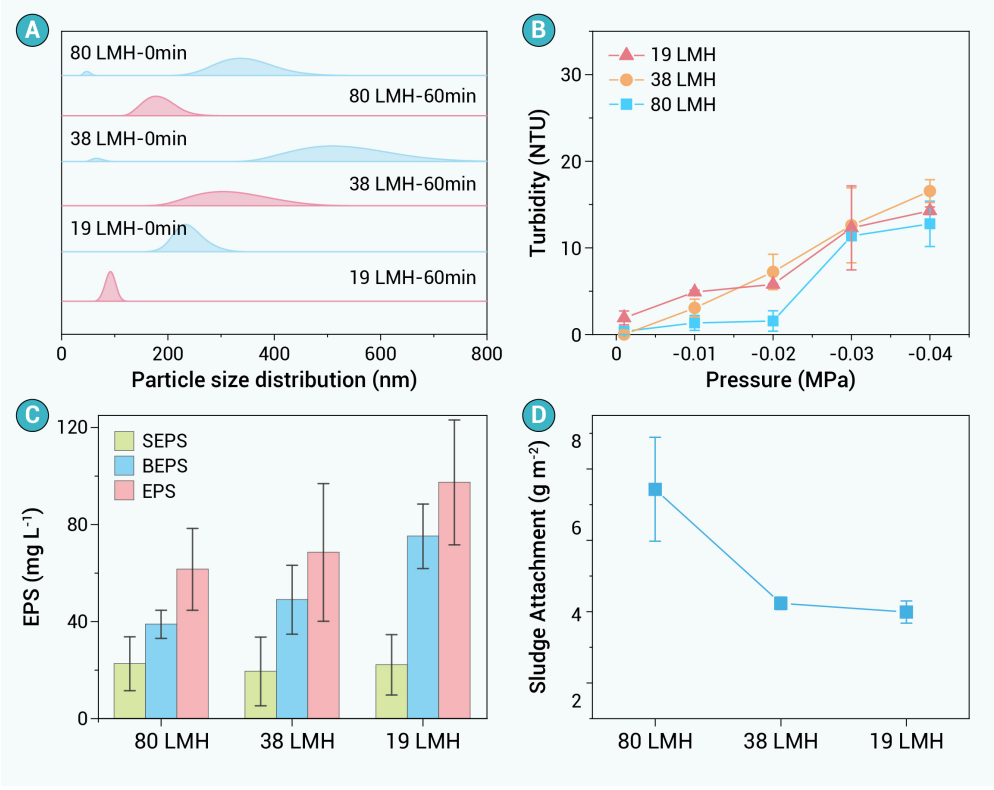

Figure 3. Pollutant rejection and sludge attachment of CTDM (A) Particle size distribution of effluent; (B) Effluent turbidity under different TMP; (C) EPS content in sludge deposits; (D) Sludge attachment on membrane surface.

two-stage stepwise scaling-up research system, including laboratory pilot-scale verification and on-site pilot-scale test. On the basis of obtaining basic parameters from the laboratory small-scale setup, the study further expanded the membrane area and reactor volume to investigate the operational stability of the medium-scale CTDM under different influent conditions (Figure 6). Using synthetic sewage, the CTDM maintained stable operation for 72 hours in the first cycle, with subsequent cycles shortened to 30±5 hours post-physical backwashing (Figure 6A). This consistency across scales confirms the technology's robustness, critical for industrial deployment. When treating domestic sewage, however, the initial cycle duration dropped to 12 hours due to elevated particulate loading (mean size: 15±3.5 μm), underscoring the need for pretreatment (Figures 6B & C). Implementing a 30-minute sedimentation step—removing >50 μm particles—extended cycle duration to 24 hours (Figure 6B), aligning with conventional MBR pretreatment protocols and demonstrating adaptability to variable feed quality. Effluent quality remained stable (Figure 6D-F): turbidity (2.8±0.3 NTU), COD removal (77.3%, 42.5 mg·L^{-1}), TP (73.3%, 1.75 mg·L^{-1}), NH_4^+-N (94.9%, 3.05 mg·L^{-1}), pH (7.0-8.2), and fecal coliforms (2.3×10^2 MPN·L^{-1}), all meeting discharge limits set by the NPDES. At 80 LMH, the large-scale CTDM system achieved 12 hours of stable operation (Figure 6E), demonstrating a 400% flux increase over traditional PM (15-20 LMH) without compromising effluent quality.

Subsequently, a long-term on-site field experiment lasting nearly 50 days was conducted in a domestic sewage treatment plant (Figure 7). The experiment was divided into three phases with filtration fluxes of 15, 25, and 75 LMH, respectively. The temporal evolution of the TMP is depicted in Figure 7A. At a flux of 15 LMH, the initial cycle operated continuously for 8 days. As the experiment proceeded, physical cleaning failed to completely remove the micro-scale foulants deeply embedded within the membrane pores, leading to a gradual reduction in the effective pore size; thereafter, each operating cycle stabilized at approximately 5 days. When operated at 25 LMH, each cycle lasted around 3 days, and all cycles exhibited a similar TMP profile. Upon increasing the flux to 75 LMH, the strong osmotic drag force accelerated the accumulation of sludge flocs on the membrane surface, resulting in a shortened operating cycle of approximately 1 day. Despite the significant fluctuation in flux, the effluent turbidity of CTDM remained consistently below 6 NTU (Figure 7A), demonstrating its excellent retention performance. Influent concentrations of indicators including COD, NH_4^+-N, TN, TP and pH fluctuated to a certain extent owing to the real domestic wastewater taken from the wastewater treatment plant; nevertheless, favorable and stable pollutant removal performance was maintained throughout the long-term experimental operation (Table S8).

In addition, this study compared the EPS contents between the membrane-attached sludge and the bulk sludge under different flux conditions (Figure 7B). The results showed that the EPS content on the membrane surface was significantly higher than that in the bulk sludge. EPS is a key factor in the formation of biofilms and also a characteristic indicator of the onset of dynamic membrane fouling. The secretion of EPS is affected by many factors. First, microbial community analysis at the phylum level (Figure S6) indicated negligible variation across the tested fluxes (15-75 LMH), demonstrating that shifts in microbial taxonomy were not the primary cause of the observed EPS variation. It is worth noting that the membrane surface EPS increased with the increase of flux in the pilot-scale experiment at the wastewater treatment plant, which was different from the conclusion of the laboratory small-scale test. This may be attributed to the physiological pressure exerted by the sheer force and high osmotic pressure induced by high flux on the microorganisms on the membrane surface under actual wastewater treatment plant conditions, stimulating them to secrete more EPS to enhance the structural stability of the biofilm.[43] Accordingly, the differences in EPS content and fouling behavior observed at different fluxes were not caused by shifts in microbial community structure, but mainly driven by hydrodynamic conditions and shear stress under elevated filtration loads.

Meanwhile, the effluent particle size was basically maintained between 100-200 nm and showed a decreasing trend with the increase of flux (Figure 7E), which was due to the denser dynamic membrane layer formed under high flux. Three-dimensional excitation-emission matrix (3D-EEM) fluorescence spectra (Figures 7C-D & F-G) showed that at the initial stage of start-up (10 min), the effluent exhibited significant fluorescent peaks of proteins and polysaccharides in the region of Ex/Em=250-280/330-380 nm;[44] with the increase of operation time, the synergistic effect of physical interception and biodegradation of the dynamic membrane layer was enhanced, and the effluent fluorescence intensity decreased, demonstrating the deep retention capacity of the mature dynamic membrane for dissolved organic matter.

Material characterization after 50 days of operation (Figure S4) demonstrated the long-term durability of CTDM. FTIR analysis showed no significant changes in the main functional groups of the membrane material (Figure S4A), while BET analysis revealed an increased specific surface area (Figure S4B), mainly attributed to the residual biofouling layer with a porous microstructure on the membrane surface after operation. XPS analysis indicated that CTDM still consisted of C and O, but their relative abundances slightly decreased (Figure S4C), presumably due to inorganic fouling of sewage-borne inorganic components (e.g., Ca, Mg) on the membrane surface, masking the chemical signals of the substrate. SEM images (Figure S4D) intuitively confirmed that the fibers remained intact, but the pore size shrank significantly due to organic/inorganic composite fouling. In addition, the contact angle increased after operation (Figure S4E), indicating enhanced membrane surface hydrophobicity, which was usually associated with the adsorption of a large amount of hydrophobic proteinaceous EPS components. The surface Zeta potential slightly decreased after operation (Figure S4F), possibly because the deposited surface layer (e.g., activated sludge with

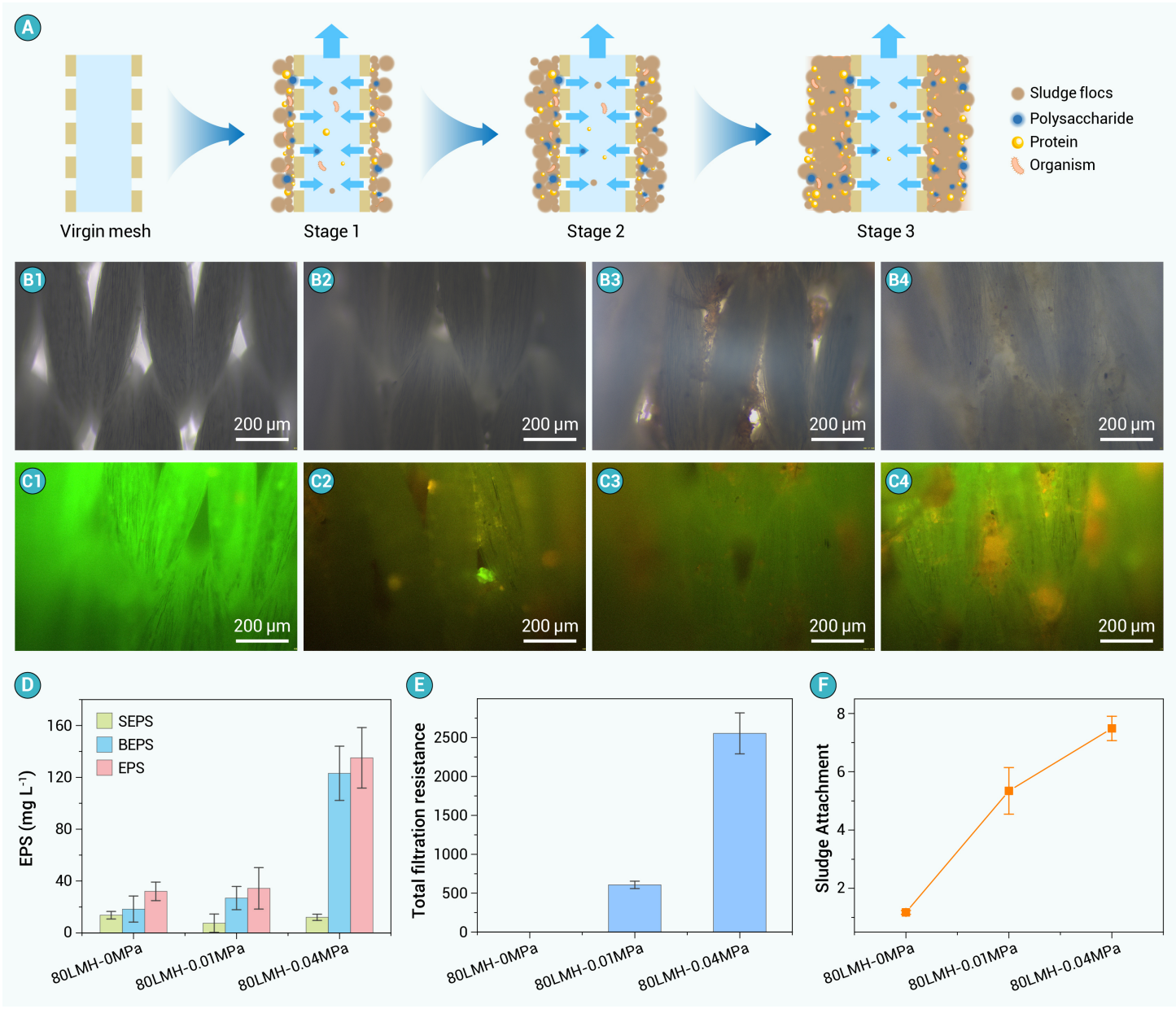

Figure 4. Formation process and mechanism of CTDM (A) Schematic of CTDM formation principle; (B1-B4) Microscopic morphology at different time points; (C1-C4) Fluorescent microscopic morphology after live/dead staining at different time points; (D) EPS content over time; (E) Sludge attachment over time; (F) Filtration resistance over time.

a Zeta potential of -3.121 mV) had weak electronegativity, masking the high electronegativity of the substrate.

The CTDM configuration represents a major advance in MBRs design by using a densely packed geometry to significantly reduce spatial constraints. As illustrated in Table 1, this innovative architecture achieves an order-of-magnitude enhancement in volumetric flux per unit footprint (10.2-fold) compared to conventional DMs, while maintaining equivalent treatment efficacy and formation kinetics. Such process intensification holds transformative potential for advancing compact water reclamation systems by decoupling performance metrics from spatial requirements.

Techno-economic analysis revealed the CTDM system's superiority over PM configurations through multiple performance vectors (Table S9). The flux enhancement from 19 to 80 LMH directly translates to a 75% reduction in required membrane area, concomitantly shrinking the MBR footprint and eliminating the need for expensive UF membrane fabrication, which substantially lowers initial hardware investment.[43] This spatial efficiency further reduces aeration energy demands proportionally, while the macroporous PP substrate mitigates pore-blocking tendencies, collectively driving down operational expenditures related to energy consumption and chemical cleaning. Although the initial start-up phase exhibits transient turbidity fluctuations, the system stabilizes rapidly to consistently meet stringent effluent quality standards, ensuring regulatory compliance. Projections based on 2011-2024 industry data and ARIMA modeling indicate that such efficiency gains will become increasingly critical as global wastewater treatment capacity expands to 2.3-fold current levels by 2035 (Figures 8B1-B3). Overall, the multi-index evaluation (Figure 8C) confirms that CTDM outperforms conventional configurations across six key metrics—including aeration energy, chemical dosage, and capital costs—validating its robust technical and economic competitiveness for next-generation wastewater treatment.

In summary, the hollow fiber CTDM system transcends the trade-offs of prior dynamic membranes, merging high flux, compact design, and operational economy. By addressing both technical and economic barriers—spatial inefficiency, fouling costs, and scalability—this technology offers a pragmatic pathway to sustainable wastewater infrastructure expansion, particularly in rapidly urbanizing regions.

Limitations and future perspectives

To advance the translation of the CTDM technology from lab-scale valida-

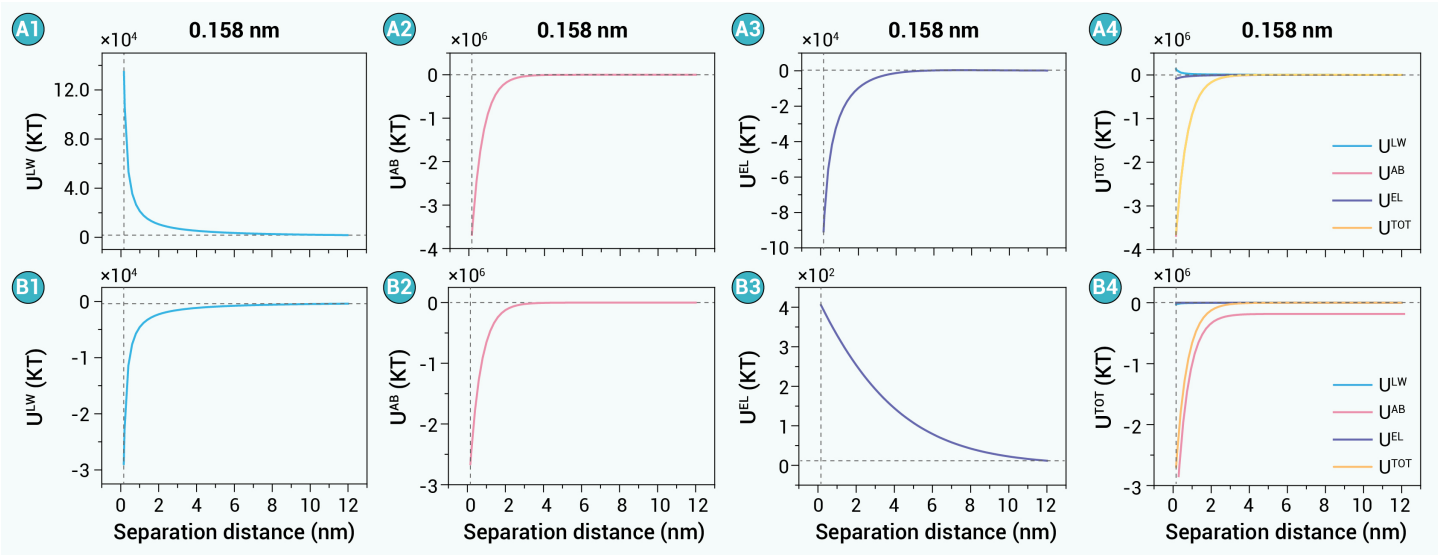

Figure 5. Interaction energy analysis based on XDLVO theory (A1-A4) Variation of U^{LW}, U^{AB}, U^{EL}, and U^{TOT} between CTDM and sludge with distance; (B1-B4) Variation of f U^{LW}, U^{AB}, U^{EL} and U^{TOT} among sludge particles with distance.

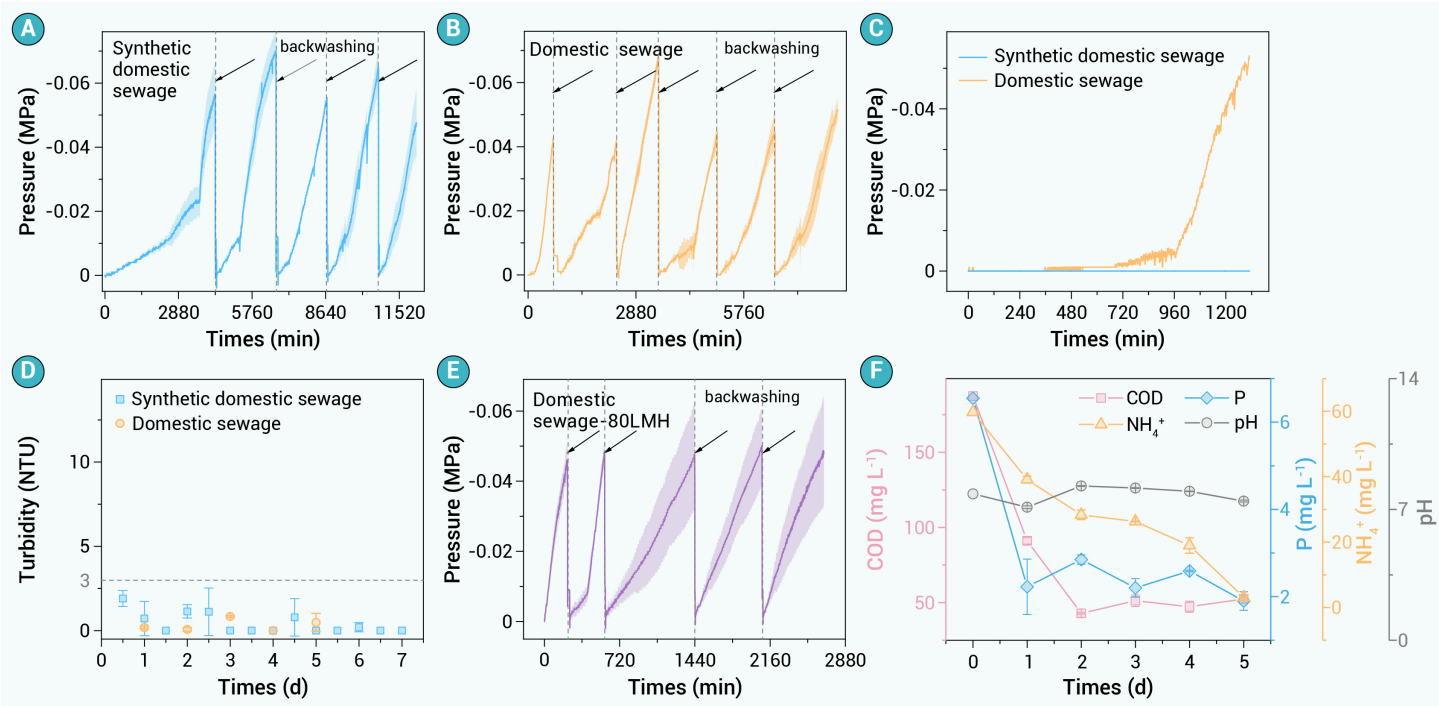

Figure 6. Operation performance of the medium-scale CTDM (A) TMP variation in synthetic domestic sewage; (B) TMP variation in domestic sewage; (C) TMP variation without activated sludge (synthetic vs. domestic sewage); (D) Effluent turbidity in synthetic and domestic sewage; (E) TMP variation at flux of 80 LMH in domestic sewage; (F) Pollutant removal performance in domestic sewage.

tion to full-scale engineering deployment, several directions warrant further exploration beyond the current proof-of-concept trials. While manual physical cleaning sufficed for controlled experimental validation, tailored automated backwashing and in-situ chemical cleaning strategies compatible with the curtain-type hollow fiber configuration are required to meet the operational demands of large-scale facilities, balancing fouling mitigation efficiency with the integrity of the functional dynamic cake layer. Brief transient turbidity elevations during the initial 10-15 min of system start-up, prior to full cake layer compaction, can be further mitigated via pre-coating or hydrodynamic optimization to shorten the water quality stabilization period for compliance with stringent discharge requirements. Although the 50-day pilot trial confirmed the structural integrity of PP fibers under typical MBR hydrodynamic conditions, extended thousand-hour-scale tests are needed to evaluate the evolution of fiber pore size and mechanical properties under persistent aeration shear and repeated cleaning cycles, supporting robust whole-life-cycle cost-benefit analyses. Notably, the interfacial interaction mechanisms quantified via XDLVO analysis herein provide a robust theoretical foundation for rational PP substrate modification—future efforts can tune surface charge density or acid-base interaction intensity to accelerate dynamic membrane formation and further suppress long-term fouling propensity. Collectively, addressing these priorities will solidify the technical and economic competitiveness of CTDM systems for next-generation MBR applications.

CONCLUSION

In this work, a polypropylene hollow fiber CTDM was developed for wastewater treatment in membrane bioreactors. The CTDM achieved a high operational flux of 80 LMH and reduced effluent turbidity to less than 5 NTU within 3 minutes, outperforming conventional PVDF membranes that only reached 15 LMH under the same conditions. Its unique structural design greatly saves

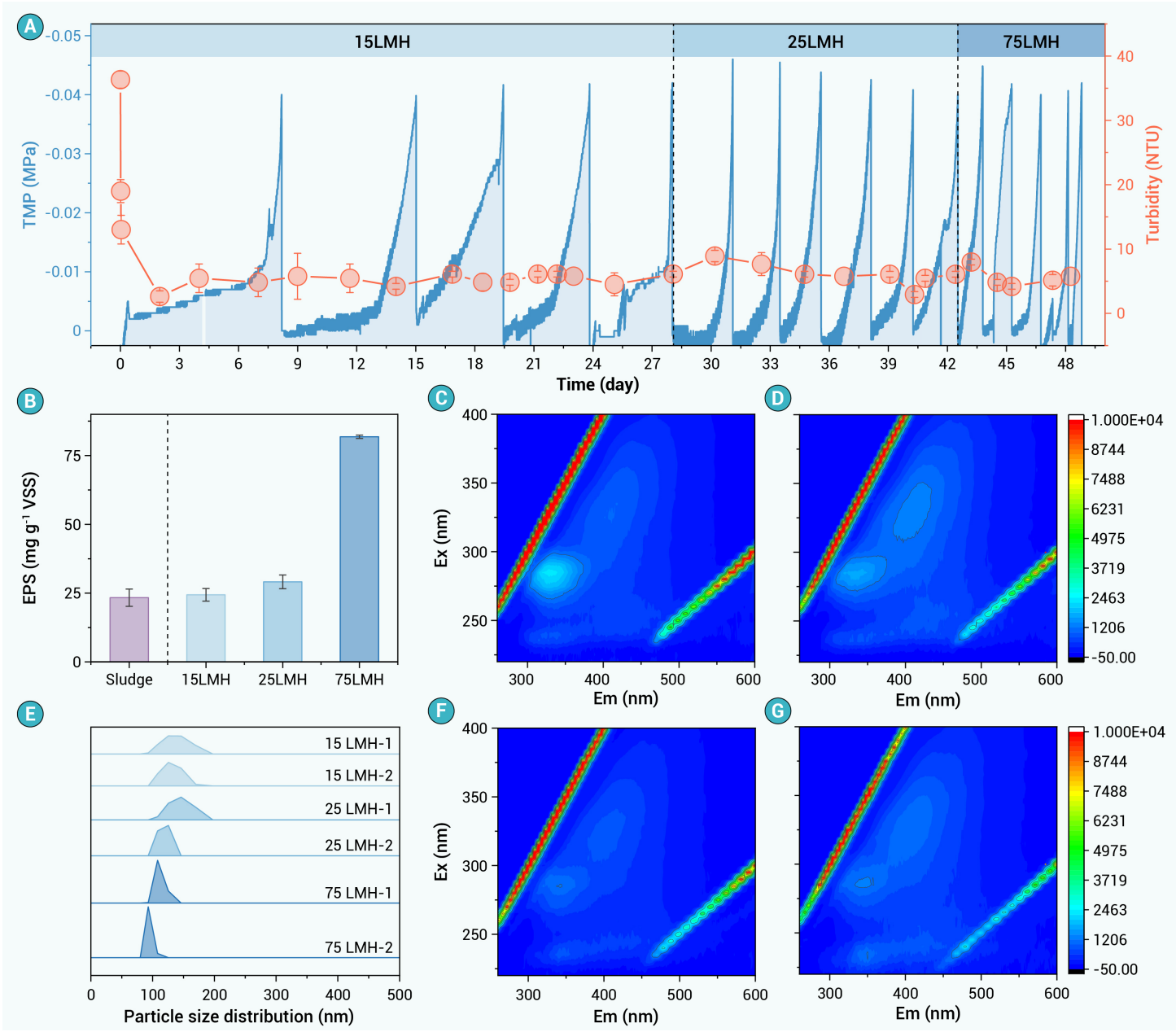

Figure 7. Operation performance of the large-scale CTDM (A) TMP and Turbidity; (B) EPS content on membrane surface; (C) 3D-EEM of effluent (10 min after startup); (D) 3D-EEM of effluent at 15 LMH; (E) Particle size distribution; (F) 3D-EEM of effluent at 25 LMH; (G) 3D-EEM of effluent at 75 LMH.

Table 1. Performance comparison of CTDM with other DMs.

Pore size (μm)	TSS ($g \cdot L^{-1}$)	Formation time	Turbidity (NTU)	COD removal rate	NH_4^+ removal rate	Flux (LMH)	Flux in the same footprint (100 m^2) ($LMH \cdot m^{-2}$)	Reference
0.39	4.2	3 d	< 2	97.5%	26.5%	4.6±0.83	0.184	Ref.[37]
2	1.5	NM	< 2	93.4%	97.2%	93±4	0.93	Ref.[24]
30	8±0.2	6-8 d	< 2	92.3%	NM	15	0.15	Ref.[6]
50	1.5	NM	< 5	90.1%	97%	93±4	0.93	Ref.[24]
70	4.2±0.5	7h	< 2	NM	NM	17	0.17	Ref.[31]
90	NM	20 min	1	NM	NM	21	0.21	Ref.[4]
300	5.8±1.7	15-45 min	< 10	NM	NM	100	1	Ref.[38]
200	3.5	< 5min	< 3	78%	94.9%	80	2.4	This study

NM: Not mentioned in the text.

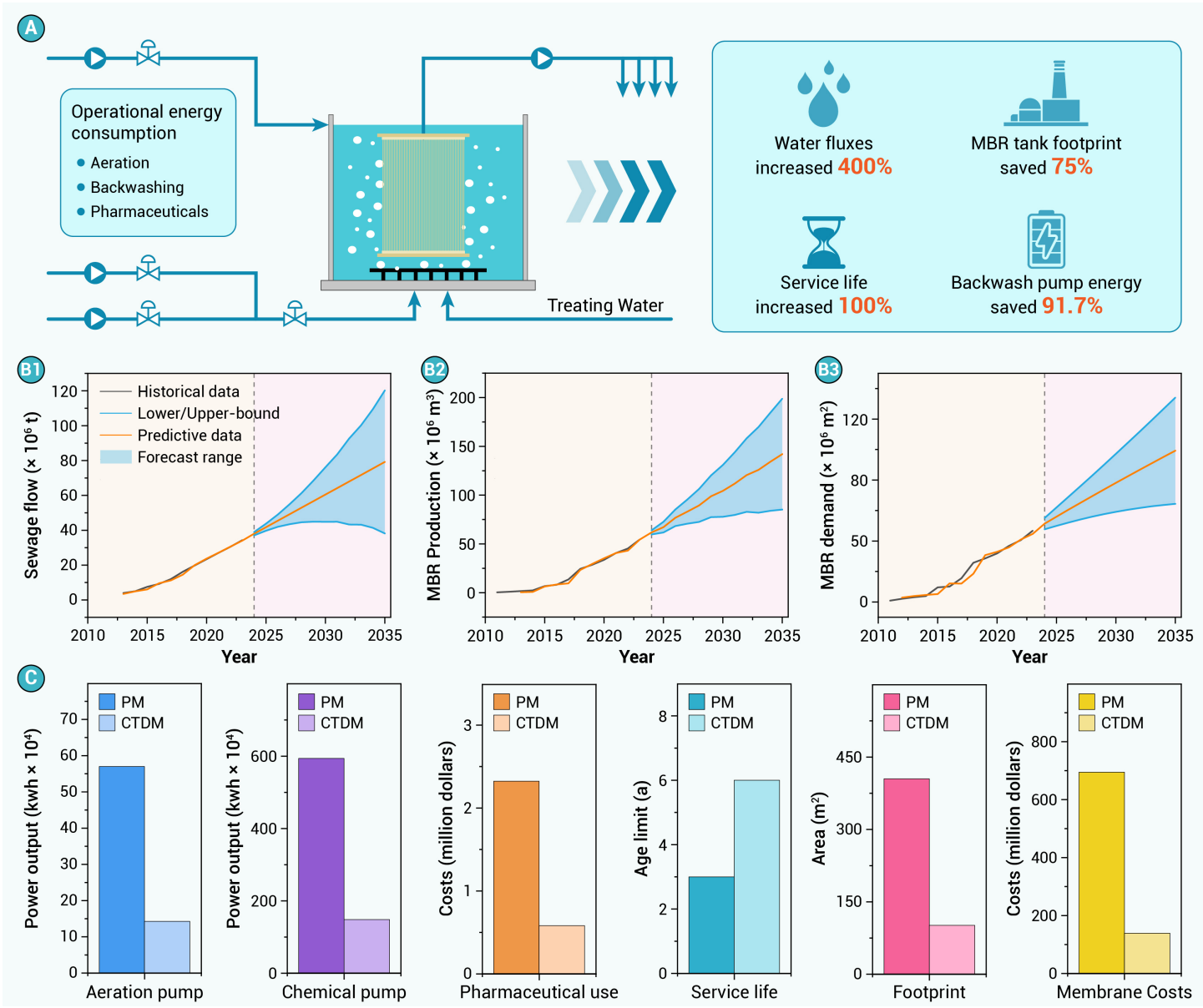

Figure 8. Techno-economic comparison between CTDM and PM (A) Schematic of economic analysis; (B1-B3) Forecasts of sewage flow, MBR production and demand (2024-2035) based on 2010-2023 data; (C) Comparison of aeration pump, chemical pump, pharmaceutical use, service life, footprint and membrane cost.

floor space and reduces the overall cost by 47.3%. The rapid formation of the CTDM is reasonably explained by the XDLVO theory. Activated sludge primarily governs filtration performance, while EPS act as the major foulant during long-term operation. As a cost-effective and high-performance alternative, this dynamic membrane technology has bright prospects for large-scale engineering application in MBR systems.

REFERENCES

1. Gharibian S. and Hazrati H. (2022). Towards practical integration of MBR with electrochemical AOP: Improved biodegradability of real pharmaceutical wastewater and fouling mitigation. *Water Res.* **218**:118478. DOI:10.1016/j.watres.2022.118478
2. Ni L., Wang P., Westerhoff P., et al. (2024). Mechanisms and strategies of advanced oxidation processes for membrane fouling control in MBRs: Membrane-foulant removal versus mixed-liquor improvement. *Environ. Sci. & Technol.* **58**:11213–11235. DOI:10.1021/acs.est.4c02659
3. He H., Xin X., Qiu W., et al. (2022). Role of nano-Fe_3O_4 particle on improving membrane bioreactor (MBR) performance: Alleviating membrane fouling and microbial mechanism. *Water Res.* **209**:117897. DOI:10.1016/j.watres.2021.117897
4. Li L., Xu G., Yu H., et al. (2018). Dynamic membrane for micro-particle removal in wastewater treatment: Performance and influencing factors. *Sci. Total Environ.* **627**:332–340. DOI:10.1016/j.scitotenv.2018.01.239
5. Fan B. and Huang X. (2002). Characteristics of a self-forming dynamic membrane coupled with a bioreactor for municipal wastewater treatment. *Environ. Sci. Technol.* **36**:5245–5251. DOI:10.1021/es025789n
6. Kizilet A., Yurtsever A., Cirik K., et al. (2022). Cake layer reformation rates on self forming dynamic membranes and performance comparison with microfiltration membranes. *Sci. Total Environ.* **838**:156384. DOI:10.1016/j.scitotenv.2022.156384
7. Cai D., Huang J., Liu G., et al. (2018). Effect of support material pore size on the filtration behavior of dynamic membrane bioreactor. *Bioresour. Technol.* **255**:359–363. DOI:10.1016/j.biortech.2018.02.007
8. Mahat S. B., Omar R., Lee J. L., et al. (2020). Effect of pore size of monofilament woven filter cloth as supporting material for dynamic membrane filtration on performance using aerobic membrane bioreactor technology. *ASIA-PAC J. Chem. Eng.* **15**:e2453. DOI:10.1002/apj.2453
9. Ersahin M. E., Ozgun H. and van Lier J. B. (2013). Effect of support material properties on dynamic membrane filtration performance. *Sep. Sci. Technol.* **48**:2263–2269. DOI:10.1080/01496395.2013.804840
10. Gilcreas F. W. (1966). Standard methods for the examination of water and waste water. *AJPH* **56**:387–388. DOI:10.2105/ajph.56.3.387
11. Bahgat N. T., Wilfert P., Eustace S. J., et al. (2024). Phosphorous speciation in EPS extracted from aerobic granular sludge. *Water Res.* **262**:122077. DOI:10.1016/j.watres.2024.122077
12. DuBois M., Gilles K. A., Hamilton J. K., et al. (1956). Colorimetric method for determination of sugars and related substances. *Anal Chem* **28**:350–356. DOI:10.1021/ac60111a017
13. Yu M., Guo W., Liang Y., et al. (2024). Towards rapid formation of electroactive

biofilm: Insights from thermodynamics and electric field manipulation. *Water Res.* **261**:121992. DOI:10.1016/j.watres.2024.121992
14. Zhang J., Xiao K., Liu Z., et al. (2021). Large-scale membrane bioreactors for industrial wastewater treatment in China: Technical and economic features, driving forces, and perspectives. *Eng.* **7**:868–880. DOI:10.1016/j.eng.2020.09.012
15. Tsuyuhara T., Hanamoto Y., Miyoshi T., et al. (2010). Influence of membrane properties on physically reversible and irreversible fouling in membrane bioreactors. *Water Sci Technol* **61**:2235–2240. DOI:10.2166/wst.2010.122
16. Liu Y., Lin B., Liu W., et al. (2018). Preparation and characterization of a novel nanofiltration membrane with chlorine-tolerant property and good separation performance. *RSC Adv.* **8**:36430–36440. DOI:10.1039/C8RA06755D
17. Szewczyk P. K., Ura D. P., Metwally S., et al. (2019). Roughness and fiber fraction dominated wetting of electrospun fiber-based porous meshes. *Polymers.* **11**:34. DOI:10.3390/polym11010034
18. Xu J., Zhang F., Xin B., et al. (2019). Application of surface wettability modified polypropylene nonwoven in Janus composite fibrous mats for the function of directional water transport. *Polym. Adv. Technol.* **30**:3038–3048. DOI:10.1002/pat.4735
19. Tao J., Song X., Bao B., et al. (2020). The role of surface wettability on water transport through membranes. *Chem. Eng.* **219**:115602. DOI:10.1016/j.ces.2020.115602
20. Cai H. H., Fan H., Zhao L. H., et al. (2016). Effects of surface charge on interfacial interactions related to membrane fouling in a submerged membrane bioreactor based on thermodynamic analysis. *J. Colloid Interface Sci.* **465**:33–41. DOI:10.1016/j.jcis.2015.11.044
21. Chen L., Lv M., Ding Y.-C., et al. (2023). Investigation of filtration performance and phosphorus removal in an electric field controlled dynamic membrane bioreactor. *Chem. Eng. J.* **478**:147328. DOI:10.1016/j.cej.2023.147328
22. Chu H., Zhang Y., Zhou X., et al. (2014). Dynamic membrane bioreactor for wastewater treatment: Operation, critical flux, and dynamic membrane structure. *J. Membr. Sci.* **450**:265–271. DOI:10.1016/j.memsci.2013.08.045
23. An Y., Wang Z., Wu Z., et al. (2009). Characterization of membrane foulants in an anaerobic non-woven fabric membrane bioreactor for municipal wastewater treatment. *Chem. Eng. J.* **155**:709–715. DOI:10.1016/j.cej.2009.09.003
24. Salerno C., Vergine P., Berardi G., et al. (2017). Influence of air scouring on the performance of a self forming dynamic membrane bioreactor (SFD MBR) for municipal wastewater treatment. *Bioresour. Technol.* **223**:301–306. DOI:10.1016/j.biortech.2016.10.054
25. Saleem M., Alibardi L., Lavagnolo M. C., et al. (2016). Effect of filtration flux on the development and operation of a dynamic membrane for anaerobic wastewater treatment. *J. Environ. Manage.* **180**:459–465. DOI:10.1016/j.jenvman.2016.05.054
26. Kiso Y., Jung Y.-J., Park M.-S., et al. (2005). Coupling of sequencing batch reactor and mesh filtration: Operational parameters and wastewater treatment performance. *Water Res.* **39**:4887–4898. DOI:10.1016/j.watres.2005.05.025
27. Xiong J., Fu D. and Singh R. P. (2014). Self-adaptive dynamic membrane module with a high flux and stable operation for the municipal wastewater treatment. *J. Membr. Sci.* **471**:308–318. DOI:10.1016/j.memsci.2014.08.001
28. Fuchs W., Resch C., Kernstock M., et al. (2005). Influence of operational conditions on the performance of a mesh filter activated sludge process. *Water Res.* **39**:803–810. DOI:10.1016/j.watres.2004.12.001
29. Rezvani F., Mehrnia M. R. and Poostchi A. A. (2014). Optimal operating strategies of SFDM formation for MBR application. *Sep. Purif. Technol.* **124**:124–133. DOI:10.1016/j.seppur.2014.01.028
30. Turken T., Sengur-Tasdemir R., Ates-Genceli E., et al. (2019). Progress on reinforced braided hollow fiber membranes in separation technologies: A review. *J. Water Process. Eng.* **32**:100938. DOI:10.1016/j.jwpe.2019.100938
31. Lv M., Feng H., Ding Y., et al. (2022). Comparison of the formation, filtration performance, and structural characteristic of self-forming dynamic membranes under constant transmembrane pressure and constant filtration flux. *J. Environ. Chem. Eng.* **10**:108691. DOI:10.1016/j.jece.2022.108691
32. Gholami M., Middelkamp B., Roy Y., et al. (2024). Flux decline in crossflow ultrafiltration-based diafiltration process for lignin recovery from a deep eutectic solvent comprised of lactic acid and choline chloride. *CHEM ENG RES DES* **202**:468–479. DOI:10.1016/j.cherd.2024.01.013
33. Liu H., Yang C., Pu W., et al. (2009). Formation mechanism and structure of dynamic membrane in the dynamic membrane bioreactor. *Chem. Eng. J.* **148**:290–295. DOI:10.1016/j.cej.2008.08.043
34. Derjaguin B. and Landau L. (1993). Theory of the stability of strongly charged lyophobic sols and of the adhesion of strongly charged particles in solutions of electrolytes. *Prog. Surf Sci.* **43**:30–59. DOI:10.1016/0079-6816(93)90013-L
35. Verwey E. J. W. and Overbeek J. T. G. (1955). Theory of the stability of lyophobic colloids. *J. Phys. Colloid Chem.* **513**:631-636. DOI: 10.1021/j150453a001
36. Feng L., Li X., Song P., et al. (2011). Surface Interactions and Fouling Properties of Micrococcus luteus with Microfiltration Membranes. *Appl. Biochem. Biotechnol.* **165**:1235–1244. DOI:10.1007/s12010-011-9341-9
37. Isik O., Abdelrahman A. M., Ozgun H., et al. (2019). Comparative evaluation of ultrafiltration and dynamic membranes in an aerobic membrane bioreactor for municipal wastewater treatment. *Environ. Sci. Pollut. R.* **26**:32723–32733. DOI:10.1007/s11356-019-04409-6
38. Elbir H., Uyanik I., Çolakoğlu E. B., et al. (2024). Pre-coating of stainless-steel mesh support material with wastewater treatment plant sludges in a dynamic membrane filtration process. *J. Water Process. Eng.* **64**:105673. DOI:10.1016/j.jwpe.2024.105673
39. Zamani F., Ullah A., Akhondi E., et al. (2016). Impact of the surface energy of particulate foulants on membrane fouling. *J. Membr. Sci.* **510**:101–111. DOI:10.1016/j.memsci.2016.02.064
40. Shen C., Zhang P., Xiang S., et al. (2025). Surface modification of PVDF membrane by physical co-deposition and bridging grafting strategy for enhanced anti-fouling performance. *Surf. Interf.* **75**:107779. DOI:10.1016/j.surfin.2025.107779
41. Huang P., Chen C., Gu M., et al. (2025). Solvation-based interfacial renovation of contaminated membranes for performance restoration and chlorine resistance enhancement. *J. Membr. Sci.* **719**:123749. DOI:10.1016/j.memsci.2025.123749
42. Li N., Zhang J., Tian Y., et al. (2016). Anti-fouling potential evaluation of PVDF membranes modified with ZnO against polysaccharide. *Chem. Eng. J.* **304**:165–174. DOI:10.1016/j.cej.2016.06.088
43. Meng F., Chae S.-R., Drews A., et al. (2009). Recent advances in membrane bioreactors (MBRs): Membrane fouling and membrane material. *Water Res.* **43**:1489–1512. DOI:10.1016/j.watres.2008.12.044
44. Chen W., Westerhoff P., Leenheer J. A., et al. (2003). Fluorescence excitation–emission matrix regional integration to quantify spectra for dissolved organic matter. *Environ. Sci. Technol.* **37**:5701–5710. DOI:10.1021/es034354c

FUNDING AND ACKNOWLEDGMENTS

This work was supported by "Leading Goose" R&D Program of Zhejiang (No. 2023C03149), the National Natural Science Foundation of China (No. 52270051), the Zhejiang Provincial Ten Thousand Plan (No. 2021R52055). The funders had no role in study design, data collection and analysis, decision to publish, or preparation of the manuscript.

AUTHOR CONTRIBUTIONS

Yanqing Zhang: Conceptualization, Methodology, Investigation, Formal analysis, Writing – original draft; **Yuxiang Liang**: Methodology, Validation, Investigation, Data curation, Writing – original draft; **Ying Chen**: Software, Validation, Formal analysis, Visualization; **Zhesong Zhou**: Resources, Investigation; **Pingli Li**: Resources, Investigation; **Dongqing Zhan**: Investigation, Validation; **Chenxuan Lou**: Investigation, Data curation; **Yangcheng Ding**: Supervision, Funding acquisition; **Yijing Xia**: Investigation, Visualization; **Wei Sun**: Resources, Formal analysis; **Yao Feng**; Methodology, Validation; **Jionghui Li**: Supervision, Project administration, Funding acquisition; **Huajun Feng**: Supervision, Project administration, Funding acquisition, Writing – review & editing. All authors contributed to the manuscript and approved the final version.

DECLARATION OF INTERESTS

The authors declare no competing interests.

DATA AND CODE AVAILABILITY

Data are available from the corresponding author upon reasonable request.

SUPPLEMENTAL INFORMATION

It can be found online at https://doi.org/10.59717/j.tiw.2026.100012.